# Revisiting the Sodiation Mechanism of TiO 2 via Operando X-ray Absorption Spectroscopy

Marcus Fehse, Aurélien Henry, Andrea Zitolo, Bruno Boury, Nicolas Louvain, Lorenzo Stievano

applied sciences

MDPI

Article

# Revisiting the Sodiation Mechanism of $TiO_2$ via *Operando* X-ray Absorption Spectroscopy

**Marcus Fehse [1,*], Aurélien Henry [2], Andrea Zitolo [3], Bruno Boury [2], Nicolas Louvain [2,4] and Lorenzo Stievano [2,4,*]**

1 CIC Energigune, Parque Tecnológico de Álava, Albert Einstein 48, ED. CIC, 01510 Miñano, Spain
2 Institut Charles Gerhardt Montpellier (ICGM), Univ. Montpellier, CNRS, 34095 Montpellier, France; aurelien.henry.mpl@free.fr (A.H.); bruno.boury@umontpellier.fr (B.B.); nicolas.louvain@umontpellier.fr (N.L.)
3 Synchrotron SOLEIL, L'orme des Merisiers, BP 48 Saint Aubin, 91192 Gif-sur-Yvette, France; andrea.zitolo@synchrotron-soleil.fr
4 Réseau sur le Stockage Electrochimique de l'Energie (RS2E), CNRS, 80039 Amiens, France
* Correspondence: marcus.fehse@umontpellier.fr (M.F.); lorenzo.stievano@umontpellier.fr (L.S.); Tel.: +34-911-922-137-365 (M.F.); +33-46714-3346 (L.S.)

Received: 30 June 2020; Accepted: 5 August 2020; Published: 11 August 2020


**Featured Application: Owing to the large availability of sodium, Na-ion batteries could be a viable and cheap alternative to Li-ion batteries, and the development of new electrode materials for this promising technology, such as $TiO_2$, is necessary to accelerate their adoption in large-scale applications.**

**Abstract:** The sodiation mechanism of $TiO_2$ anatase was thoroughly investigated via X-ray absorption spectroscopy under *operando* conditions. The data set was analysed via an innovative and smart approach based on chemometric tools that allows the unbiased and reliable extraction of the maximum amount of meaningful information. The resulting data analysis reveals that the electrochemical sodiation mechanism is mainly based on the reduction of $Ti^{4+}$ to $Ti^{3+}$, going along with the irreversible amorphisation of the pristine anatase structure. At least one semi-amorphous intermediate is formed during the first discharge, whose local structure resembles those obtained at the end of the charge.

**Keywords:** $TiO_2$; anatase; sodium-ion batteries; X-ray absorption spectroscopy; chemometrics

## 1. Introduction

$TiO_2$ has gained considerable interest as negative electrode material in lithium-ion batteries due to its stable cycling and inherently safe insertion potential [1,2]. While the latter is preserved for its reaction towards sodium, the underlying redox mechanism is clearly distinct from the lithium insertion reaction [3–5]. Nevertheless, stable electrochemical cycling with high reversibility has been obtained for the sodiation reaction of anatase, the most redox-active $TiO_2$ polymorph, which continues to nourish performance-orientated research interest [6–11].

At the same time, the precise reaction mechanism on which this remarkable performance is based is still not completely understood. In practice three different mechanisms have been proposed for the electrochemical sodiation of $TiO_2$ anatase: (i) the redox reaction based on the $Ti^{4+}/Ti^{3+}$ with no phase change, (ii) the redox reaction based on $Ti^{4+}/Ti^{3+}$ with the intermediate formation of an amorphous phase, and (iii) a complete conversion reaction mechanism implying the formation of metal Ti nanoparticles [5]. For instance, while Kim et al. [12] simply proposed the reversible intercalation of sodium ions in anatase, Passerini and coworkers suggested a much more complex mechanism

implying the disproportionation of an intermediate sodium titanate phase into a mixture of new phases including Ti metal and amorphous titanate during the first discharge process, the latter phase being responsible for the further cycling activity of the material [4]. Their findings are largely supported by those of Ding et al., although differing sample and experimental conditions limit comparability [13]. To unveil the structural changes and phase transitions and propose such mechanisms, many different ex situ and in a few cases in situ techniques have been applied. Among them, the widely applied X-ray diffraction (XRD) has proven to be insufficient to closely follow the reaction mechanism, due to the loss of long-range order upon first sodiation. This has lead to ambiguous claims causing much debate. As a result short-range probing techniques such as Raman spectroscopy and synchrotron based pair distribution function were carried out under *operando* conditions to provide more reliable insights from a local structural perspective [14,15]. Based on these findings an amorphous $Na_xTiO_2$ phase appears to form in the initial sodiation reaction. Upon desodiation amorphisation aggravates and an "anatase-like" amorphous structure is recovered. These two phases build the foundation for the reversible redox mechanism.

X-ray absorption spectroscopy (XAS) has proven to be particularly useful for analysis of complex reaction mechanism which are accompanied by strong nanostructuring upon electrochemical cycling [16]. Thanks to its element specificity, the needlessness for long-range order and the high penetration of x-rays, it provides reliable bulk information on the electronic and local structure of the absorbing element. In the specific case of anatase vs. sodium, Kim et al. applied it ex situ to follow the evolution of the oxidation state of Ti [12]. In their case, the evolution of the X-ray Absorption Near Edge Structure (XANES) of the XAS and in particular the edge position proved the reversible reduction of part of the $Ti^{4+}$ to $Ti^{3+}$ during the discharge and its oxidation upon charging, thus excluding the occurrence of a conversion reaction which would have implied the formation of titanium metal nanoparticles [17]. More recently, ex situ XAS was applied by Passerini and coworkers to follow the sodiation of anatase nanoparticles [18]. By studying the Extended X-ray Absorption Fine Structure (EXAFS) of the XAS spectra, they propose a rearrangement of the coordination sphere of titanium leading to 5-coordinated Ti. However, their pristine material could not be simply interpreted by assuming only the presence of the anatase structure. Moreover, only a few spectra of the material at the end of the charge/discharge processes were collected, which therefore could not provide a comprehensive and complete picture of the reaction mechanism.

In this study, *operando* Ti K-edge XAS was applied to study the electrochemical sodiation/desodiation mechanism of $TiO_2$ anatase. The obtained results were processed and analysed via an innovative and reliable chemometric approach. In fact, XAS fulfils the bilinearity requirements needed for the application of chemometric tools such as Principal Component Analysis (PCA) and Multivariate Curve Resolution-Alternating Least Squares (MCR-ALS) for the data analysis. Such a method permits the fast and reliable extraction of maximum amount of meaningful data from a large data set, often allowing the detection of elusive intermediates and transient phases and their evolution through the whole reaction mechanism [19].

## 2. Results

$TiO_2$ anatase electrode was mounted in special electrochemical cell and cycled vs. Na while XAS spectra on Ti K-edge were acquired, as described in Section 5. The evolution of the XANES portion of the XAS dataset along with corresponding electrochemical cycling curve is shown in Figure 1. In particular, the inset in (a) depicts the evolution of the pre-edge features. In the spectrum of the pristine electrode, the pre-edge shows the typical features of anatase structure consisting of 4 peaks commonly labelled A1, A2, A3 and B, and resulting from the octahedral coordination geometry of titanium in the anatase structure [20].

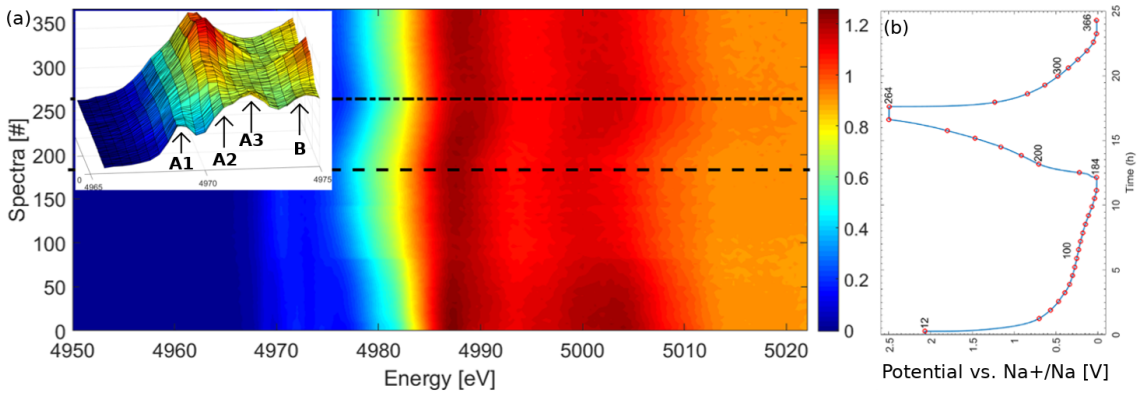


**Figure 1.** (**a**) Evolution of *operando* Ti K-edge XANES of $TiO_2$ anatase electrode vs. Na. Dashed line indicates the end of first discharge (#184) and dashed-dotted line the end of charge (#264). The inset shows the evolution of the four indicated pre-edge features $A_1$, $A_2$, $A_3$ and B in the range from 4965 to 4975 eV. (**b**) Corresponding electrochemical cycling curve of the first 1,5 electrochemical cycles of $TiO_2$ vs. Na.

During the sodiation, a shift of the Ti K-edge position to lower energies is observed, reflecting the reduction of $Ti^{4+}$ to $Ti^{3+}$ which demonstrates the redox activity of the $Ti^{4+/3+}$ redox couple, in line with previous ex situ findings [12,18]. Simultaneously, a slight increase of the intensity of the A2 pre-edge peak and a general fading of the other features is observed, which has been attributed to the aggravating distortion of the coordination of the Ti centres with respect to crystalline $TiO_2$ [18,21]. A similar change in the shape of the pre-edge was already observed in the case of the lithiation of anatase [22,23]. It is noteworthy that, while the main edge position seems to be largely reversed upon desodiation, the changes in the pre-edge features are not, indicating, differently from the case of lithium, that non-reversible structural rearrangements have occurred upon initial sodiation.

The complete dataset comprising more than 350 XAS spectra was analysed via Principal Component Analysis revealing the existence of four independent component (see Appendix A, Figure A1). This rank analysis results paired with additional chemical and physical constrains was used as input for MCR-ALS tool which resulted in pure components whose spectra and concentration profile are presented in Figure A2 (cf. Appendix A) and Figure 2, respectively.

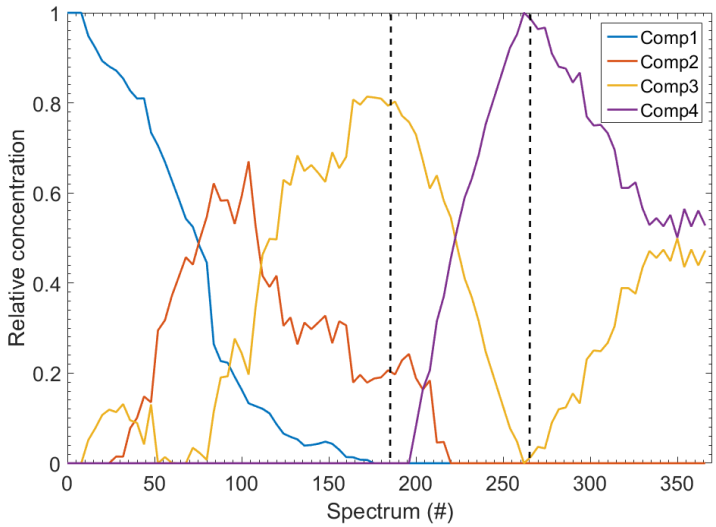


**Figure 2.** Concentration profile of pure spectral components obtained through MCR-ALS during 1.5 electrochemical cycles of $TiO_2$ vs. Na. The dashed lines indicate end of first discharge (#184) and end of first charge (#264).

From the evolution of the concentration of the four pure components, several perceptions can be made. Component #1 is the sole component at the onset of electrochemical cycling and therefore represents the pristine state. Its intensity quickly decreases upon sodiation and does not increase upon inversion of current (charge). This suggests that the pristine state is not recovered after the first complete electrochemical cycle, which reminds of conversion-type anode materials [24]. Instead of a reemerging component #1, a new component #4 is formed during desodiation and reaches its maximum at the end first charge corresponding to the completion of one full electrochemical cycle (spectrum #264). Even though component #3 is dominant at the end of first discharge (spectrum #184), a 20% contribution of component #2 is still present. The latter has a transient nature, as it reaches its maximum intensity about half-way through the discharge reaction and then fades gradually as sodiation continues.

To gain insights on the local structure of the absorbing Ti at specific points of the electrochemical reaction, the EXAFS signal of the pure components was fitted and structural parameters about the nature of next neighbouring shells extracted (cf. Figure 3 and Table 1, respectively). A comparison of the EXAFS signal in k-space of the MCR-ALS pure spectral components with selected experimental spectra shows good agreement and reduced noise level for MCR-ALS which improves fitting accuracy, see Figure A3. Component #1 can be fitted in quite straightforward manner based on the published structure of $TiO_2$ anatase [25], using a simple single scattering approach. Best fitting agreement was achieved when including two elongated bonds in the first oxygen shell, in agreement with the typical axially elongated octahedral coordination of titanium in anatase [18,25].

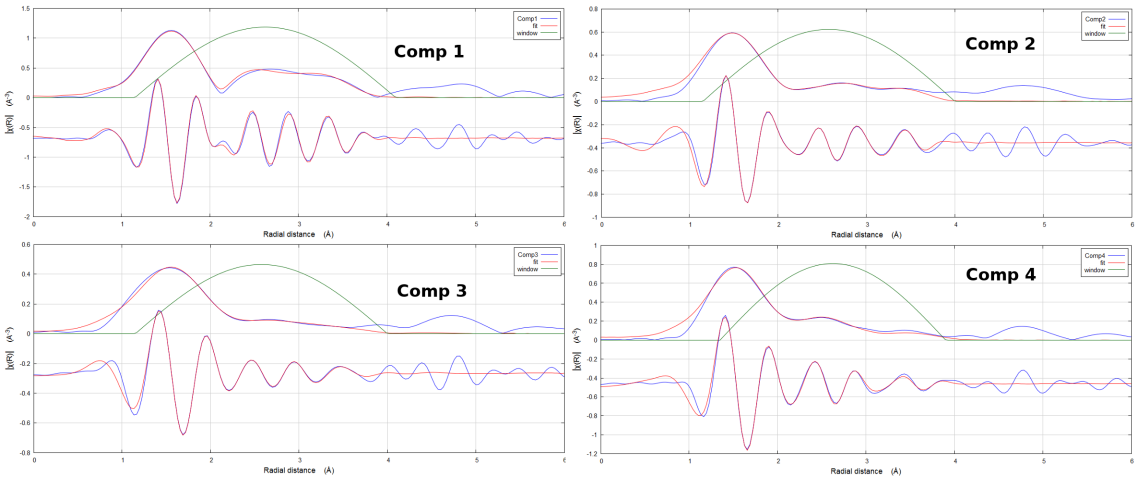


**Figure 3.** Fourier transform of EXAFS signal in R-space of the four MCR-ALS pure components (blue). Top curve in each plot corresponds to magnitude and bottom curve to real-part contribution. Fit of the real-space EXAFS signal (red) and the range in which the fit was carried out (green).

Analogous to Component #1, a first coordination shell with similar configuration (two different bond lengths with respective populations of 4 + 2 neighbours) is also observed for the other three components. The bond lengths values of Components #2 are very similar to those of Component #1, but they become more elongated for component #3, corresponding to the completely reduced sample at the end of the first discharge (EOD). On the other hand, the bond distances decrease again for Component #4, which corresponds to the sample after one complete discharge/charge cycle (EOC), even though they do not reach the values of the initial state. Our findings suggest that the initial state is not recovered after one electrochemical cycle. This is in good agreement with the absence of anatase features reformation upon desodation and irreversible crystal structural rearrangements evinced in an in situ XRD study by Wu and coworkers [4]. Going from Component #1 to #3, a noticeable increase of the Debye-Waller factors is observed for both shells, in line with a gradual increase of the disorder and the presence of larger distributions of bond lengths for increasingly sodiated species.

Comparing Component #3 and #4, the Debye-Waller factors of the first two shells decrease slightly, reaching values similar to those obtained for Component #2.

For the three outer shells, similar bond length as for pristine state are found, within the error range. A rise in bond length and of the Debye-Waller $\sigma^2$ factors is observed with increasing sodiation, reflecting the rise of disorder upon sodium uptake. It should be noted that due their practically identical electronic structure, sodium and oxygen neighbours are virtually impossible to distinguish by EXAFS. Therefore the outer shell of component 4 has been marked as "Ti-Na ($O_3$)" to account for this ambiguity, see Table 1.

**Table 1.** Ti K-edge EXAFS fitting parameters of MCR-ALS components.

| Component | Shell | N * | $R_{fit}$ [Å] | $\sigma^2$ [Å]$^2$ |
|---|---|---|---|---|
| MCR #1 | Ti-$O_1$ | 4 | 1.91(1) | 0.0014(6) |
| | Ti-$O_2$ | 2 | 2.32(2) | 0.0014(6) |
| | Ti-$Ti_1$ | 4 | 3.02(8) | 0.008(1) |
| | Ti-$Ti_2$ | 4 | 3.87(8) | 0.008(1) |
| | Ti-$O_3$ | 8 | 3.79(3) | 0.004(10) |
| MCR #2 | Ti-$O_1$ | 4 | 1.91(1) | 0.008(1) |
| | Ti-$O_2$ | 2 | 2.33(1) | 0.008(1) |
| | Ti-$Ti_1$ | 6 | 3.09(3) | 0.022(3) |
| | Ti-Na | 3 | 3.20(3) | 0.005(2) |
| | Ti-$Ti_2$ | 3 | 3.89(3) | 0.012(2) |
| MCR #3 | Ti-$O_1$ | 4 | 2.00(2) | 0.014(1) |
| | Ti-$O_2$ | 2 | 2.47(2) | 0.014(1) |
| | Ti-$Ti_1$ | 4 | 3.18(3) | 0.018(3) |
| | Ti-Na | 3 | 3.34(4) | 0.015(4) |
| | Ti-$O_2$ | 6 | 3.98(5) | 0.024(5) |
| MCR #4 | Ti-$O_1$ | 4 | 1.97(1) | 0.007(1) |
| | Ti-$O_2$ | 2 | 2.41(2) | 0.007(1) |
| | Ti-$Ti_1$ | 4 | 3.07(3) | 0.013(2) |
| | Ti-$Ti_2$ | 2 | 3.98(3) | 0.013(2) |
| | Ti-Na ($O_3$) | 3 | 3.85(3) | 0.023(3) |

* Amplitude reduction factor was evaluated for pure anatase at the value of 0.8, and then kept fixed for all fits. Coordination numbers were evaluated and then kept fix for the presented fit.

## 3. Discussion

These findings, and in particular the similarities between components #2 and #4, suggest that, in the first part of the discharge, the incipient sodiation induces the formation of a reaction intermediate via the amorphisation of the starting crystalline anatase structure. This partially sodiated species characterised by a local "$TiO_2$-like" structure, is recovered after one complete electrochemical cycle, in agreement with the findings of previous pair distribution function (PDF) analysis [15].

Component #3, which corresponds to the majority component present at EOD was fitted based on the structure of delafossite ($NaTiO_2$, ICSD 68872) taking into account a partial occupancy of the Na site of 0.5. In this way, it was possible to obtain an adequate fit, with bond distances very similar to those reported for this structure. Noteworthy are the elevated Debye-Waller factors which indicate a highly disordered semi-amorphous structure. This is well in line with previous findings of a disordered $Na_xTiO_2$ phase prevailing at complete sodiation state [14,15].

The intermediate Component #2 and #4, on the contrary, could be fitted with the structure derived from $TiO_2$ anatase. However, the introduction of a additional Na-O neighbours was necessary to achieve a satisfactory fit. This intermediate component can hence be understood as an amorphous anatase-like structure containing a non negligible fraction of sodium. Making such transient species visible is one of the assets of the chemometrics supported *operando* XAS analysis [19].

Our results also rebut the formation of metallic titanium upon conversion of the initial anatase, as previously proposed by Wu et al. [4] These authors could detect the formation of Ti metal by ex situ X-ray photoelectron spectroscopy (XPS). Considering that such measurements are obtained with the samples submitted to high vacuum conditions, it is conceivable that the slightly reducing conditions in the XPS analysis chamber have induced the further reduction of $Ti^{3+}$ to titanium metal in the near surface region.

A simplified sum, without mass balance, of the reaction mechanism for the sodiation of $TiO_2$ anatase based on our and previous studies results can hence be written as follows:

$$TiO_2 + x\text{Na} \xrightarrow{1\text{st}sodiation} \text{“Na}_x\text{TiO}_2\text{”} \xleftrightarrow{Subsequent\ cycle} \text{“TiO}_2\text{”} + \text{“Na}_x\text{TiO}_2\text{”} + \text{Na} \quad (1)$$

where as the quotation marks indicate highly disordered and or amorphous “$TiO_2$” and “$Na_xTiO_2$” phases whose local structure are anatase and delafossite-like.

## 4. Conclusions

The application of *operando* XAS to the study of the sodiation/desodiation mechanism of anatase confirmed, in line with previously published studies, that the electrochemical sodiation mechanism occurs via the reduction of $Ti^{4+}$ to $Ti^{3+}$. This reduction occurring with the insertion of sodium produces an amorphisation of the pristine anatase structure, which is not recovered upon charge. At least one intermediate semi-amorphous species is produced during the first discharge, which is not very different from the species obtained at the end of the charge. Based on the obtained *operando* results, the occurrence of a conversion reaction during the discharge leading to the formation of highly reactive titanium metal nanoparticles can be excluded.

## 5. Materials and Methods

### *5.1. Material Synthesis and Electrode Formulation*

Mesoporous $TiO_2$ anatase was obtained as previously reported [14]. In short, titanium tetraisopropoxide (Sigma-Aldrich, 0.032 mol) and glacial acetic acid (VWR Chemicals, 0.016 mol) were dissolved in 20 mL absolute ethanol and stirred for 12 h. The solution was then added dropwise to 100 mL deionized water under vigorous stirring, and subsequently aged for 1 h. The powder was recovered by centrifugation and dried in vacuo overnight at 100 °C and calcined in air at 400 °C for 1 h to yield mesoporous $TiO_2$.

Self-supported electrodes were made from an aqueous slurry containing $TiO_2$ active material, carbon black and sodium carboxymethyl cellulose binder in the ratio 60:12:28 with a loading of $\approx 3\,mg\,cm^{-2}$. Electrodes with such a specifically tailored loading were necessary for the *operando* XAS analysis, in order to obtain an optimised signal-to-noise ratio in the measured spectra. The mixture was thoroughly mixed in a planetary ball-mill for 1 h, tape-casted on a thin aluminium foil (thickness ≈ 10 µm), dried at room temperature and subsequently at 100 °C in vacuo.

### *5.2. Operando X-ray Absorption Spectroscopy*

XAS measurements at the Ti K-edge was performed in the fluorescence mode at the *SAMBA* beamline of Synchrotron *SOLEIL* in Gif-sur-Yvette (France). A focusing double-crystal Si(220) monochromator was used. The *operando* electrochemical cell [26], was placed after a ionisation chamber needed to measure the intensity of the incident beam with an angle of 45 ° with respect to the latter. XAS spectra were collected continuously for the first cycle and a half (discharge/charge/discharge) with a cycling rate of C/10, where 1 C corresponds to the reaction of 1 mol of Na with 1 mol of $TiO_2$.

In the XANES (X-ray absorption near-edge structure) region of Ti K-edges (4966 eV), equidistant energy steps of E = 0.4 eV were used. For all measured spectra, the exact energy calibration was established with simultaneous absorption measurements on a Ti reference pellet placed between the

second and the third ionisation chamber. In the EXAFS (Extended X-ray Absorption Fine Structure) region, data were collected up to k = 12 $Å^{-1}$.

The operando XAS spectra were first globally analysed by a statistical tool named Principal Component Analysis (PCA), employing the Singular Value Decomposition (SVD) algorithm with the computer program `Matlab`. The number of principal components determined in this way was used as the basis for Multivariate Curve Resolution-Alternating Least Squares (MCR-ALS) analysis, which allows the stepwise reconstruction of the spectral components which are necessary for interpreting the whole multiset of operando spectra. The whole procedure is described in detail in ref. [19]. The MCR-ALS analysis was performed with the following constraints: (i) 100 non-negativity of the intensity and of the concentration of the components, (ii) no unimodality and (iii) closure (sum of the components always equal to 100 % of the intensity). The reconstructed pure spectral components were extracted and fitted using the `IFEFFIT` software package [27]. Fourier transform of EXAFS oscillations with different $k$ weights was carried out in $k$-range from 2.5 to 11.0 $Å^{-1}$. Fitting was performed in R-range from 1.4 to 3.65 Å using $k^2$ and $k^3$ weights. EXAFS amplitudes and phase-shifts were calculated by `FEFF` starting from the calculated lattice parameters of $TiO_2$. Interatomic distances (R) and the Debye-Waller factors ($\sigma^2$) were calculated for all paths included in the fits.

**Author Contributions:** Conceptualization, N.L. and L.S.; methodology, A.Z. and L.S.; validation, B.B., N.L. and L.S.; formal analysis, M.F. and L.S.; investigation, A.Z., A.H. and L.S.; resources, B.B., N.L. and L.S.; data curation, M.F. and L.S.; writing—original draft preparation, M.F.; writing—review and editing, all authors; visualization, all authors; supervision, L.S.; project administration, B.B. and N.L.; funding acquisition, B.B., N.L. and L.S. All authors have read and agreed to the published version of the manuscript.

**Funding:** This research received no external funding.

**Acknowledgments:** Synchrotron SOLEIL is acknowledged for providing beamtime at beamline SAMBA (proposal number 20151085). Spanish Ministerio de Ciencia e Innovación is acknowledged for its support through the project ION-SELF (ref. PID2019-106519RB-I00). Antonella Iadecola (RS2E) is gratefully acknowledged for technical and logistic help in the preparation of the measurement session at the synchrotron. Last but not least, the authors are in debt to Laure Monconduit (ICGM) for continuously providing valuable professional input and fruitful discussion throughout the length of this study.

**Conflicts of Interest:** The authors declare no conflict of interest.

## Abbreviations

The following abbreviations are used in this manuscript:

| | |
|---|---|
| EOC | End of Charge |
| EOD | End of Discharge |
| EXAFS | Extended X-ray Absorption Fine Structure |
| MCR-ALS | Multivariate Curve Resolution - Alternating Least Squares |
| PCA | Principal Component Analysis |
| PDF | Pair Distribution Function |
| XANES | X-ray Absorption Near-Edge Structure |
| XAS | X-ray Absorption Spectroscopy |
| XPS | X-ray Photoelectron Spectroscopy |
| XRD | X-ray Diffraction |

## Appendix A

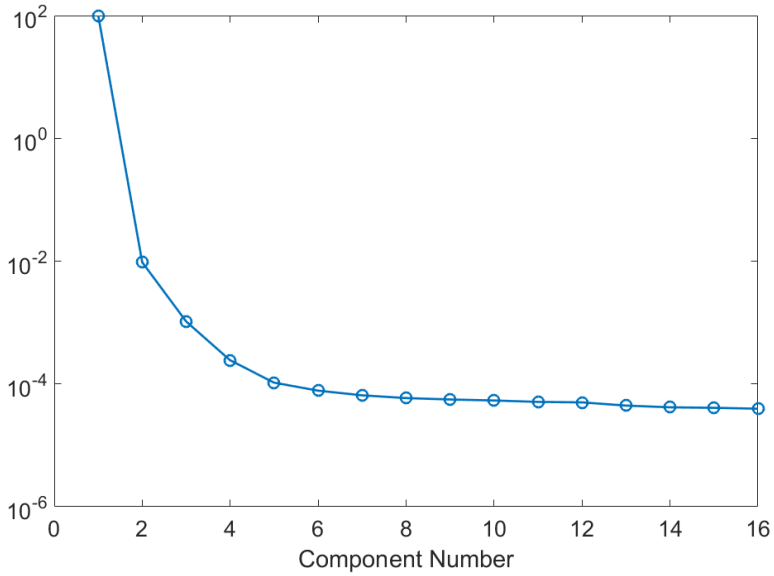


**Figure A1.** Variance distribution of eigenvalues obtained via PCA. It Four components make up the majority of variance, all subsequent can be considered as representing experimental noise.

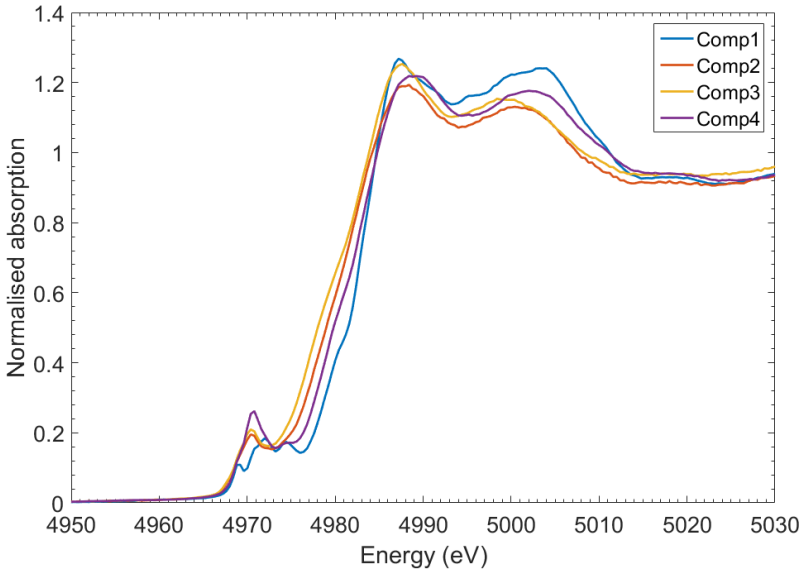


**Figure A2.** XANES portion of pure spectral components obtained through MCR-ALS applied to operando Ti k-edge data set. The comparison shows shift of edge position to lower energies upon sodiation as well its partial recovery upon desodiation.

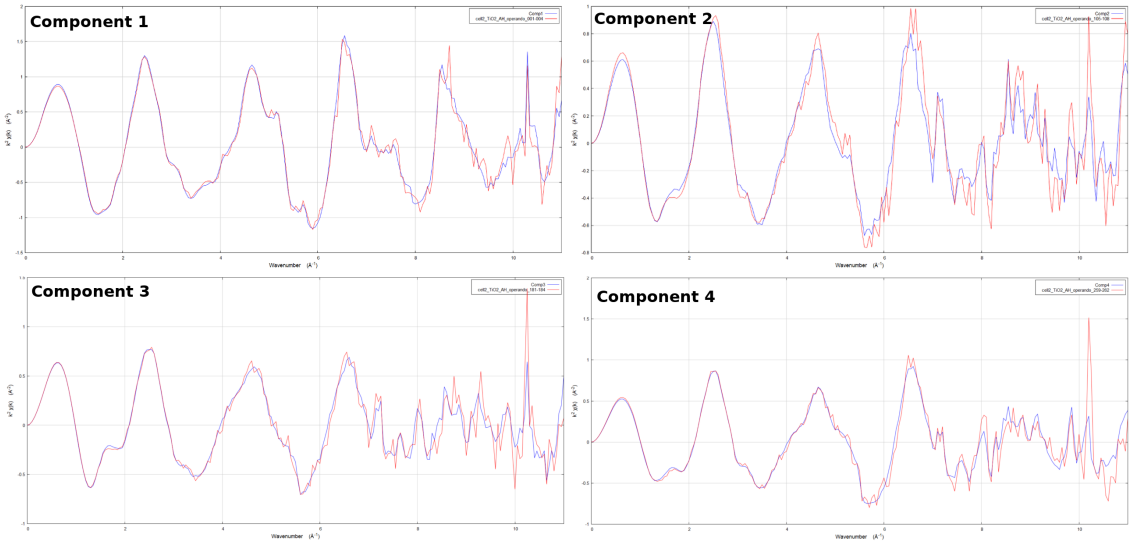


**Figure A3.** Comparison of EXAFS signal in k-space of MCR-ALS pure components (blue) and selected experimental spectra (red).The noise reduction for the MCR-ALS pure components compared to experimental spectra is salient.

## References


1. Ge, M.; Cao, C.; Huang, J.; Li, S.; Chen, Z.; Zhang, K.Q.; Al-Deyab, S.S.; Lai, Y. A review of one-dimensional TiO2 nanostructured materials for environmental and energy applications. *J. Mater. Chem. A* **2016**, *4*, 6772–6801. [CrossRef]
2. Fehse, M.; Ventosa, E. Is TiO2(B) the future of titanium-based battery materials? *ChemPlusChem* **2015**, *80*, 785–795. [CrossRef] [PubMed]
3. Guo, S.; Yi, J.; Sun, Y.; Zhou, H. Recent advances in titanium-based electrode materials for stationary sodium-ion batteries. *Energy Environ. Sci.* **2016**, *9*, 2978–3006. [CrossRef]
4. Wu, L.; Bresser, D.; Buchholz, D.; Giffin, G.A.; Castro, C.R.; Ochel, A.; Passerini, S. Unfolding the Mechanism of Sodium Insertion in Anatase TiO2 Nanoparticles. *Adv. Energy Mater.* **2015**, *5*, 1401142. [CrossRef]
5. Lou, S.; Zhao, Y.; Wang, J.; Yin, G.; Du, C.; Sun, X. Ti?Based Oxide Anode Materials for Advanced Electrochemical Energy Storage: Lithium/Sodium Ion Batteries and Hybrid Pseudocapacitors. *Small* **2019**, *15*, 1904740. [CrossRef] [PubMed]
6. Wu, L.; Buchholz, D.; Bresser, D.; Gomes Chagas, L.; Passerini, S. Anatase $TiO_2$ nanoparticles for high power sodium-ion anodes. *J. Power Sources* **2014**, *251*, 379–385. [CrossRef]
7. Su, D.; Dou, S.; Wang, G. Anatase $TiO_2$: Better Anode Material Than Amorphous and Rutile Phases of $TiO_2$ for Na-Ion Batteries. *Chem. Mater.* **2015**, *27*, 6022–6029. [CrossRef]
8. Chen, C.; Wen, Y.; Hu, X.; Ji, X.; Yan, M.; Mai, L.; Hu, P.; Shan, B.; Huang, Y. Na(+) intercalation pseudocapacitance in graphene-coupled titanium oxide enabling ultra-fast sodium storage and long-term cycling. *Nat. Commun.* **2015**, *6*, 6929. [CrossRef]
9. Chen, J.; Ding, Z.; Wang, C.; Hou, H.; Zhang, Y.; Wang, C.; Zou, G.; Ji, X. Black Anatase Titania with Ultrafast Sodium-Storage Performances Stimulated by Oxygen Vacancies. *ACS Appl. Mater. Interfaces* **2016**, *8*, 9142–9151. [CrossRef] [PubMed]
10. Ling, L.; Bai, Y.; Wang, Z.; Ni, Q.; Chen, G.; Zhou, Z.; Wu, C. Remarkable Effect of Sodium Alginate Aqueous Binder on Anatase TiO2 as High-Performance Anode in Sodium Ion Batteries. *ACS Appl. Mater. Interfaces* **2018**, *10*, 5560–5568. [CrossRef]
11. Ni, Q.; Dong, R.; Bai, Y.; Wang, Z.; Ren, H.; Sean, S.; Wu, F.; Xu, H.; Wu, C. Superior sodium-storage behavior of flexible anatase TiO2 promoted by oxygen vacancies. *Energy Storage Mater.* **2020**, *25*, 903–911. [CrossRef]
12. Kim, K.T.; Ali, G.; Chung, K.Y.; Yoon, C.S.; Yashiro, H.; Sun, Y.K.; Lu, J.; Amine, K.; Myung, S.T. Anatase titania nanorods as an intercalation anode material for rechargeable sodium batteries. *Nano Lett.* **2014**, *14*, 416–422. [CrossRef] [PubMed]

13. Ding, C.; Nohira, T.; Hagiwara, R. A new sodiation-desodiation mechanism of the titania-based negative electrode for sodium-ion batteries. *Phys. Chem. Chem. Phys.* **2016**, *18*, 30770–30776. [CrossRef] [PubMed]
14. Louvain, N.; Henry, A.; Daenens, L.; Boury, B.; Stievano, L.; Monconduit, L. On the electrochemical encounter between sodium and mesoporous anatase TiO 2 as a Na-ion electrode. *CrystEngComm* **2016**, *18*, 4431–4437. [CrossRef]
15. Li, W.; Fukunishi, M.; Morgan, B.J.; Borkiewicz, O.J.; Chapman, K.W.; Pralong, V.; Maignan, A.; Lebedev, O.I.; Ma, J.; Groult, H.; et al. A Reversible Phase Transition for Sodium Insertion in Anatase TiO2. *Chem. Mater.* **2017**, *29*, 1836–1844. [CrossRef]
16. Fehse, M.; Sougrati, M.T.; Darwiche, A.; Gabaudan, V.; La Fontaine, C.; Monconduit, L.; Stievano, L. Elucidating the origin of superior electrochemical cycling performance: New insights on sodiation-desodiation mechanism of SnSb from: Operando spectroscopy. *J. Mater. Chem. A* **2018**, *6*, 8724–8734. [CrossRef]
17. Cabana, J.; Monconduit, L.; Larcher, D.; Palacín, M.R. Beyond Intercalation-Based Li-Ion Batteries: The State of the Art and Challenges of Electrode Materials Reacting Through Conversion Reactions. *Adv. Mater.* **2010**, *22*, E170–E192. [CrossRef]
18. Greco, G.; Mazzio, K.A.; Dou, X.; Gericke, E.; Wendt, R.; Krumrey, M.; Passerini, S. Structural Study of Carbon-Coated TiO2 Anatase Nanoparticles as High-Performance Anode Materials for Na-Ion Batteries. *ACS Appl. Energy Mater.* **2019**, *2*, 7142–7151. [CrossRef]
19. Fehse, M.; Iadecola, A.; Sougrati, M.T.; Conti, P.; Giorgetti, M.; Stievano, L. Applying chemometrics to study battery materials: Towards the comprehensive analysis of complex operando datasets. *Energy Storage Mater.* **2019**, *18*, 328–337. [CrossRef]
20. Matsuo, S.; Sakaguchi, N.; Wakita, H. Pre-edge features of Ti K-edge X-ray absorption near-edge structure for the local structure of sol-gel titanium oxides. *Anal. Sci.* **2005**, *21*, 805–809. [CrossRef]
21. Wan, J.; Chen, W.; Jia, C.; Zheng, L.; Dong, J.; Zheng, X.; Wang, Y.; Yan, W.; Chen, C.; Peng, Q.; et al. Defect Effects on TiO2 Nanosheets: Stabilizing Single Atomic Site Au and Promoting Catalytic Properties. *Adv. Mater.* **2018**, *30*, 1705369. [CrossRef] [PubMed]
22. Lafont, U.; Carta, D.; Mountjoy, G.; Chadwick, A.V.; Kelder, E.M. In Situ Structural Changes upon Electrochemical Lithium Insertion in Nanosized Anatase $TiO_2$. *J. Phys. Chem. C* **2010**, *114*, 1372–1378. [CrossRef]
23. Fehse, M.; Monconduit, L.; Fischer, F.; Tessier, C.; Stievano, L. Study of the insertion mechanism of lithium into anatase by operando X-ray diffraction and absorption spectroscopy. *Solid State Ionics* **2014**, *268*, 252–255. [CrossRef]
24. Fehse, M.; Darwiche, A.; Sougrati, M.T.; Kelder, E.M.; Chadwick, A.V.; Alfredsson, M.; Monconduit, L.; Stievano, L. In-Depth Analysis of the Conversion Mechanism of TiSnSb vs Li by Operando Triple-Edge X-ray Absorption Spectroscopy: A Chemometric Approach. *Chem. Mater.* **2017**, *29*, 10446–10454. [CrossRef]
25. Horn, M.; Schwebdtfeger, C.F.; Meagher, E.P. Refinement of the structure of anatase at several temperatures. *Z. Kristallogr.* **1972**, *136*. [CrossRef]
26. Leriche, J.B.; Hamelet, S.; Shu, J.; Morcrette, M.; Masquelier, C.; Ouvrard, G.; Zerrouki, M.; Soudan, P.; Belin, S.; Elkaïm, E.; et al. An electrochemical cell for operando study of lithium batteries using synchrotron radiation. *J. Electrochem. Soc.* **2010**, *157*, A606–A610. [CrossRef]
27. Ravel, B.; Newville, M. ATHENA, ARTEMIS, HEPHAESTUS: Data analysis for X-ray absorption spectroscopy using IFEFFIT. *J. Synchrotron Rad.* **2005**, *12*, 537–541. [CrossRef]